

Remarkable self-degradation of Cu/SAPO-34 selective catalytic reduction catalysts during storage at ambient conditions

Aiyong Wang,^a Ying Chen,^b Eric D. Walter,^b Nancy M. Washton,^b Tamas Varga,^b Yilin Wang,^a János Szanyi,^a Yong Wang,^{a,c} Charles H.F. Peden,^a Feng Gao^{a,*}

^a Institute for Integrated Catalysis, Pacific Northwest National Laboratory, P.O. Box 999, Richland, WA 99354, United States

^b Environmental Molecular Sciences Laboratory, Pacific Northwest National Laboratory, P.O. Box 999, Richland, WA 99354, United States

^c School of Chemical Engineering and Bioengineering, Washington State University, Pullman, WA 99164, United States

Abstract:

A model Cu/SAPO-34 SCR catalyst with all Cu species maintained as isolated Cu(II) ions is synthesized. Following lengthy storage on the shelf under ambient conditions, this catalyst completely and irreversibly deactivates upon any heat treatments above ~100 °C. Via detailed characterizations with surface area/pore volume analysis, XRD, H₂-TPR, and ²⁷Al, ²⁹Si and ³¹P solid-state NMR, as well as continuous wave and pulsed EPR studies, it is concluded that over the course of storage, the SCR active sites [Cu(OH)]⁺ and Brønsted acid sites ≡Si-O(H)-Al≡ are attacked by H₂O molecules trapped in the SAPO-34 framework pores, and undergo extensive hydrolysis to form copper hydroxide and terminal Al sites. Upon thermal treatment, these species interact with each other to form copper-aluminate-like species, leading to irreversible deactivation of this catalyst. This deactivation mechanism does not require or necessarily lead to extensive degradation (i.e., crystallinity loss) of the SAPO-34 support.

Keywords: SCR, ammonia, Cu-exchanged zeolite, SAPO-34, catalyst deactivation

*: corresponding author (feng.gao@pnnl.gov)

1. Introduction

As one of the two commercial selective NO_x catalytic reduction (SCR) catalysts by NH₃ used in vehicle diesel engine exhaust aftertreatment systems, Cu/SAPO-34 has been extensively studied in recent years [1-16]. This silicoaluminophosphate molecular sieve-based catalyst offers a few advantages in comparison to its aluminosilicate zeolite-based counterpart, Cu/SSZ-13: higher high-temperature hydrothermal stability [17-19], lower selectivity to unwanted N₂O formation [18], and, in particular, lower synthesis cost. The latter is due primarily to the fact that the structure directing agent (SDA) for SSZ-13 synthesis, trimethyladamantylammonium hydroxide, is much more costly than SDAs for SAPO-34 synthesis (e.g., morpholine or triethylamine). However, a major drawback for Cu/SAPO-34 has been identified in the past few years, i.e., its irreversible deactivation in the presence of moisture at near-ambient temperatures (< 100 °C) [15, 16, 19].

It is well known that the SAPO-34 framework hydrolyzes and loses crystallinity, sometimes irreversibly, in the presence of water vapor below 100 °C [20, 21]. The SDAs used to synthesize SAPO-34 were found to correlate with this type of water sensitivity; SAPO-34 materials synthesized using SDAs that lead to lower framework charge densities, e.g., tetraethyl ammonium hydroxide and triethyl amine, are more stable than materials synthesized with SDAs that lead to higher framework charge densities, e.g., morpholine [20, 21]. Since framework charges are associated with ≡Si-O(H)-Al≡ moieties in SAPO materials, this leads naturally to a hypothesis that instability of SAPO-34 is initiated with ≡Al-O(H)-Si≡ hydrolysis, e.g., $\equiv\text{Si-O(H)-Al}\equiv + 3\text{H}_2\text{O} \rightleftharpoons \equiv\text{Si-OH} + \equiv\text{Al(H}_2\text{O)}_3$. Note that this hydrolysis chemistry causes transformation of framework Si from Q₄ (i.e., Si(OT)₄) into Q₃ (Si(OT)₃(OH)) coordination, and tetrahedrally coordinated framework Al into octahedrally coordinated Al; the observation of these species via NMR spectroscopy readily corroborates occurrence of this hydrolysis chemistry [5, 20, 21]. When

SAPO-34 materials are only exposed to water vapor for short periods, the hydrolysis reaction described above can be fully reversible [20]; however with longer exposures, continuous hydrolysis lead to the generation of Q_2 ($Si(OT)_2(OH)_2$) and Q_1 ($Si(OT)(OH)_3$) Si, and eventually free $Si(OH)_4$. Upon formation of each $Si(OH)_4$, 4 terminal Al species (3 hydrated $\equiv Al-OH$ and 1 hydrated $\equiv Al$) form [22]. These latter hydrolysis steps, known as desilication, cause irreversible structural degradation of the SAPO-34 framework.

The low-temperature degradation of Cu/SAPO-34 in the presence of moisture is obviously more complicated, involving both decay of the support, and deactivation of the copper active species. How the SCR active Cu species deactivate during such reversible and irreversible support hydrolysis described above, is only beginning to be understood. In a 2015 study, Leistner and Olsson prepared two Cu/SAPO-34 catalysts with Cu loadings of 1.27 and 2.60 wt.% (SAPO-34 synthesized using morpholine as SDA and Cu addition via solution ion-exchange), and treated them with water vapor (5%) at 70 °C for various durations. These catalysts severely deactivated with only ~10 hours of such treatments. Based on the much more severe SCR activity losses than surface area/pore volume losses, the authors suggested that the SCR activity loss is caused by a transformation of the active copper sites into an inactive form [15]. Unfortunately in this publication, the authors did not specify how this transformation occurs, nor for the nature of this “inactive form”. In a more recent study, the same group further investigated the effect of SDA on low-temperature Cu/SAPO-34 deactivation, where SAPO-34 supports were synthesized with triethyl amine, tetraethyl ammonium hydroxide and morpholine SDAs, Cu was introduced via incipient wetness impregnation, and the catalysts were then degreened at 700 °C. The authors discovered that Cu/SAPO-34 catalysts more resistant to water attack are prepared with SAPO-34 supports more resistant to water. Based on catalyst characterizations using multiple spectroscopic

and chemical titration methods, the authors also suggested that the SDA of choice also influences Cu location, which may be important for understanding catalyst deactivation.

Wang et al.[16] reported also in 2015 that low temperature water-induced deactivation of Cu/SAPO-34 can be circumvented by synthesizing catalysts with high Cu loadings. The authors synthesized their catalysts using a “one-pot” approach, where morpholine was chosen as the SDA and tetraethylenepentamine (TEPA) was used as a complexing agent for Cu(II) ions. The freshly prepared, calcined catalysts were held at 70 °C for 60 h in an atmosphere of 80% relative humidity. The SAPO-34 support itself completely decomposed following this treatment; catalysts with 0.35 and 1.70% Cu loadings partially decomposed; however catalysts with 3.91 and 6.78% Cu loadings remained intact. Cu loadings of 3.91 and 6.78% are not practical for commercial SCR catalyst synthesis since catalysts with such high Cu contents will most certainly lose their high-temperature hydrothermal stability [14, 23-25]. Importantly, however, the authors discovered that the low temperature moisture-resistant catalysts contain roughly the same isolated Cu contents of ~2.3 %. Note that this value corresponds to ~0.8 isolated Cu-ion per hexagonal unit cell of the support ($T_{36}O_{72}$). Therefore, it can be suggested that even for a relatively vulnerable SAPO-34 material made using morpholine as SDA, as long as the majority of unit cells are “protected” by isolated Cu ions, the entire material can still be highly moisture-resistant. More recently, Cao et al. [26] also studied the effects of hydration treatments to low-temperature Cu/SAPO-34 stability. The catalyst used here was synthesized using diethyl amine as SDA, and 1.14 wt% Cu was introduced via solution ion-exchange prior to SDA combustion, which the authors called direct ion-exchange. Interestingly, the authors reported that cyclic hydration-dehydration treatment is more destructive than continuous hydration treatment.

In short, the studies described above collectively provide important new insights into the low temperature, water-induced Cu/SAPO-34 degradation. However, a detailed mechanistic-level understanding of this low-temperature deactivation has been missing in these studies. Only very recently, via comprehensive studies involving reaction kinetics, spectroscopies (in particular 2-dimensional electron paramagnetic resonance) and density functional theory calculations, we for the first time proposed that this degradation process involves hydrolysis chemistries of both isolated Cu-ions and the SAPO-34 framework, leading eventually to the conversion of SCR active Cu-ions to SCR inert, Cu-aluminate-like species [27]. In the present study, we provide more experimental details further corroborating this catalyst degradation proposal.

2. Experimental methods

The “one-pot” Cu/SAPO-34 catalyst presented in this study was synthesized using a method similar to that used by Prakash and Unnikrishnan [28] for the synthesis of pure SAPO-34, except for Cu addition into the gel for the current case. A Cu-TEPA complex solution, prepared by mixing 5 g of anhydrous CuSO₄, 6 g of tetraethylenepentamine (TEPA) and 89 g of deionized water, was used as the Cu source. This complex has been shown to be stable during SAPO-34 synthesis, which can also serve as a co-structure directing agent (co-SDA) [1, 29]. Morpholine was chosen as the primary SDA. Previous studies have shown that this SDA leads to SAPO-34 materials relatively vulnerable to water attack [19, 20]. This characteristic is not ideal for applications, but benefited this study of Cu/SAPO-34 degradation. 85% o-phosphoric acid (H₃PO₄) was used as the P source; aluminum hydroxide powder (containing ~54% Al₂O₃) was used as the Al source, and fumed silica (0.001 μm particle size) was used as the Si source. All chemicals used in our syntheses were purchased from Sigma-Aldrich, with purities of analytical grade or better. Synthesis gel molar composition was the following: 0.038 Cu-TEPA: 2 SDA: 0.9 SiO₂: 0.83 P₂O₅: 1 Al₂O₃: 60 H₂O.

The detailed synthesis procedure was as follows: (1) o-phosphoric acid and deionized water were first mixed and stirred for 5 min at room temperature. (2) Aluminum hydroxide powder was then slowly added in 5 min under stirring; the slurry was then stirred for 20 min. (3) Fumed silica was added within 10 min and the slurry was stirred for 30 min. (4) Morpholine was added drop by drop under stirring and the slurry was then stirred for 30 min. (5) The Cu-TEPA solution, measured to contain the desired amount of Cu, was slowly added to the slurry under stirring. (6) The suspension was transferred to a 150 ml PTFE lined autoclave containing a magnetic stir bar and sealed. The autoclave was placed above a stir/heat plate and inside a sand bath. Under stirring (500 rpm), the slurry was aged at room temperature for 24 h to facilitate silica hydrolysis. Subsequently, the sand bath temperature was raised to 200 °C in order to start SAPO-34 crystallization. The synthesis was maintained for 48 h under continuous stirring, and then the sand bath was cooled down to room temperature. (7) The solid product was separated with centrifugation, washed twice with deionized water, and then dried at 120 °C in flowing N₂ before calcination in static air at 600 °C for 5h to burn off the SDA. Cu loading of 0.71 wt% and Al/P/Si atomic ratio = 2.5/1.7/1.0 (Si/(Al+P+Si) = 0.19) of the catalyst (after SDA removal) were determined with Inductively Coupled Plasma Atomic Emission Spectroscopy (ICP-AES) conducted at Galbraith Laboratories (Knoxville, TN, USA); these values are consistent with the synthesis gel composition.

The freshly calcined catalyst is designated as Cu-F, where “F” stands for “fresh”. A portion of the fresh catalyst was stored in glass vial under typical laboratory environments (~20 °C, relative humidity ~50%) for 240 days. This sample is named Cu-S, where “S” stands for “stored” sample. Note that in the as-prepared (i.e., prior to calcination to remove SDA) form, the catalyst has high structural stability during storage (i.e., XRD patterns show no variation with time). As will be shown below, this is no longer the case after calcination to remove SDA. Therefore, all

characterizations and reaction tests of the fresh catalyst, Cu-F, were conducted within days after its calcination.

Ex situ powder X-Ray diffraction (XRD) was performed on a PANalytical X'Pert MPD system with a vertical Θ - Θ goniometer (190-mm radius). The X-ray source is a long-fine-focus, ceramic X-ray tube with a Cu anode, operating at 40 kV and 50 mA. The data were collected with 2θ ranging from 5 to 50° using a step size of 0.02°. In situ XRD was performed on a PANalytical X'Pert MPD system with a vertical Θ - Θ goniometer (220 mm radius). The X-ray source was a long-fine-focus, ceramic X-ray tube with a Cu anode, operating at 45 kV and 40 mA. The sample was placed on a sample stage (Anton Paar HTK 1200, temperature range 20–1000 °C) and heated stepwise in dry N₂ flow from 20 °C to higher temperatures at 20 °C intervals. At each temperature, scanning was conducted from 10 to 50° with a step size of 0.02°.

Surface areas (BET method) and micropore volumes (t-plot method) of the samples were measured with a Quantachrome Autosorb-6 analyzer. Prior to measurements, the samples were dehydrated under a vacuum overnight at 250 °C. As will be shown below, Cu-S loses its crystallinity after this treatment.

Temperature-programmed reduction with H₂ (H₂-TPR) was performed on a Micromeritics AutoChem II analyzer. After purging the hydrated samples (samples stored in air and saturated with moisture) with pure N₂ at 10 mL/min at room temperature for 30 min, TPR was carried out in 5% H₂/Ar at a flow rate of 30 mL/min. Temperature was ramped linearly from ambient to 650 °C at 10 K/min, and H₂ consumption was monitored with a TCD detector. H₂ consumption was quantified using Ag₂O and CuO standards.

Electron paramagnetic resonance (EPR) experiments were carried out on a Bruker E580 X-band spectrometer. Powder samples (~15 mg) were contained in 4 mm OD quartz tubes. For

continuous wave (CW) experiments it is equipped with a SHQE resonator and a continuous flow cryostat. During spectral acquisition, microwave power was 200 mW, and the frequency was 9.86 GHz. The field was swept 1500 G in 84 s and modulated at 100 kHz with a 5 G amplitude. A time constant of 20 ms was used. The isolated Cu(II) contents were quantified using the following method. Typically, spectra acquired at 125 K were first double-integrated to obtain signal areas, which are proportional to EPR active isolated Cu(II) contents. To quantify these, a series of standard solutions with different isolated Cu(II) concentrations were prepared by dissolving $\text{Cu}(\text{NO}_3)_2 \cdot 2.5\text{H}_2\text{O}$ and imidazole (Sigma Aldrich, 99%) in ethylene glycol (Sigma Aldrich, 99.8%). Imidazole was used here to coordinate with Cu(II) ions to prevent formation of EPR silent Cu dimers. The linear calibration curve generated using the integral areas and Cu contents of the standard solutions was then used for quantification of isolated Cu(II) in the catalysts. For pulsed EPR experiments the spectrometer was outfitted with an MD-5 dielectric resonator and an Oxford liquid helium continuous flow cryostat which maintained the temperature at 10 K. Typical parameters for hyperfine sublevel correlation (HYSCORE) experiments with a $\pi/2$ - τ - $\pi/2$ - t_1 - π - t_2 - $\pi/2$ sequence were: $\pi/2 = 8$ ns, $\pi = 16$ ns, $\tau = 128$ ns and t_1, t_2 ranging from 200 ns to 2248 ns in 128 steps of 16 ns. The recycle delay was ~ 500 us and typically 1024 shots were collected for each delay.

Nuclear magnetic resonance (NMR) experiments were performed on powder samples either fully hydrated or after evacuation at 10^{-3} Torr and 150 °C for 12 h (dehydrated). All experiments were conducted under a dry N_2 atmosphere. ^{27}Al and ^{31}P direct polarization (DP) experiments were carried out on a Varian VNMRs system operating at 14.1 T utilizing a 4 mm TR probe operating in DR mode. Direct polarization experiments with ^1H decoupling were conducted utilizing a ^1H frequency of 599.8517, continuous wave decoupling fields of 45 kHz for both ^{27}Al and ^{31}P , and

^{27}Al and ^{31}P frequencies of 156.3056 and 242.8129, respectively. Calibrated $\pi/20$ pulses of 0.50 μs , spinning frequency of 15 kHz, a 50 kHz spectral window, 2048 complex points, and a 2 s pulse delay were utilized to acquire 512 time-averaged scans for ^{27}Al DP experiments. Time domain free induction decays were apodized with exponential functions corresponding to 200 Hz of Lorentzian line broadening prior to Fourier transformation. A $\pi/2$ pulse of 5.0 μs , a spinning frequency of 15 kHz, 100 kHz spectral window, 4096 complex points, and a 240 s pulse delay were utilized to acquire 4 time averaged scans for ^{31}P DP experiments. Time domain free induction decays were apodized with exponential functions corresponding to 100 Hz of Lorentzian line broadening prior to Fourier transformation. ^{29}Si DP experiments were carried out on a Varian VNMRS system operating at 20 T utilizing a 4 mm TR probe operating in DR mode. Direct polarization experiments with ^1H decoupling were conducted utilizing a ^1H frequency of 849.7299 and a continuous wave decoupling field of 50 kHz. A total of 640 time-averaged transients were acquired utilizing a $\pi/2$ pulse of 6.0 μs at a ^{29}Si frequency of 168.8018, spinning frequency of 10 kHz, a 50 kHz spectral window, 5024 complex points, and a 120 s pulse delay. Time domain free induction decays were apodized with exponential functions corresponding to 300 Hz of Lorentzian line broadening.

NH_3 -SCR reaction was measured using a plug flow reaction system described elsewhere [30]. Powder samples were pressed, crushed and sieved (60-80 mesh) prior to use. For standard SCR, the feed gas contained 360 ppm NO, 360 ppm NH_3 , 14% O_2 , 2.5% H_2O and balance N_2 . H_2O was introduced to the feed by passing balance gas N_2 through a water saturator. All of the gas lines were maintained at ~ 120 $^\circ\text{C}$ to avoid water condensation. The total gas flow was 1000 sccm. For “light-off” experiments, 200 mg catalyst was used, and the gas hourly space velocity (GHSV) was estimated to be $\sim 200,000$ h^{-1} . For low-temperature kinetic studies, NO_x and NH_3 conversions were

maintained low (<15%). In this case, 60 mg catalyst was used, resulting in a GHSV of ~650, 000 h⁻¹. Concentrations of reactants and products were measured by an online MKS 2030 FTIR analyzer. Prior to reaction testing, the catalysts were first pretreated in a 14% O₂/N₂ flow for 1h at 500 °C. The following equations were used to calculate NO_x and NH₃ conversions:

$$NO_x \text{ conversion}\% = \frac{(NO + NO_2)_{inlet} - (NO + NO_2 + N_2O)_{outlet}}{(NO + NO_2)_{inlet}} \times 100$$

$$NH_3 \text{ conversion}\% = \frac{(NH_3)_{inlet} - (NH_3)_{outlet}}{(NH_3)_{inlet}} \times 100$$

3. Results and Discussion

At the onset of this section, it is important to note that the catalyst used in the present study was prepared for the purpose of elucidating low-temperature instability of Cu/SAPO-34 in the presence of moisture, rather than for practical SCR applications. Therefore, “simplicity” was weighted more than “durability” in designing this catalyst. Morpholine was chosen here since this SDA is known to lead to SAPO-34 materials with relatively low stability [5, 19, 20]. Additionally, Si content of the gel was chosen high and Cu content was chosen low in order for the SAPO-34 support to have sufficient Brønsted acid sites to host all Cu as isolated Cu(II) ions. The BET surface area of Cu-F is 364 m²/g and the micropore volume is 0.204 cm³/g, and the XRD pattern demonstrates a pure Chabazite (CHA) phase for the catalyst (not shown). Through elemental analysis via ICP, the fresh catalyst contains 0.71% Cu. The isolated Cu(II) content of the catalyst, as provided by EPR analysis [31], is 0.70%. The similarity between these two values demonstrates that essentially all Cu in the fresh catalyst is present as isolated Cu(II) ions. Thus, Cu-F is indeed successfully prepared, owing considerable simplicity to facilitate investigations on Cu-ion transformation and catalyst deactivation.

Figure 1 presents standard SCR performance of the Cu-F and Cu-S samples by comparing their NO_x and NH_3 light-off curves. Cu-F displays the expected performance, reaching $\sim 100\%$ NO_x conversions at temperatures ≥ 200 °C. This sample is also highly selective for SCR as evidenced by the similar NO_x and NH_3 conversions at all reaction temperatures tested here. This is consistent with the fact that this catalyst is essentially CuO free. CuO is known not to be selective for SCR; rather, it effectively catalyzes NH_3 oxidation ($4\text{NH}_3 + 3\text{O}_2 = 2\text{N}_2 + 6\text{H}_2\text{O}$) at ~ 300 °C and above [23, 32]. In contrast, the Cu-S sample is much less active, achieving NO_x conversions no higher than 20% at any reaction temperature. Furthermore, this catalyst becomes less selective for SCR at reaction temperatures above ~ 300 °C, suggesting that it contains CuO, or other Cu moieties that are more selective to NH_3 oxidation than SCR.

The SCR performance of Cu-S shown above is rather surprising, suggesting that great changes may have occurred during storage of Cu-F. To obtain insights into the possible changes, XRD and EPR were used to probe Cu-S in its hydrated ambient state (i.e., prior to any additional treatment). Interestingly, the sample not only maintains the CHA structure, but also maintains 0.51 wt% EPR active Cu (i.e., isolated Cu(II)). These results are inconsistent with such a dramatic SCR performance loss as shown in Figure 1, suggesting that some marked changes of this catalyst may have occurred during SCR testing. Indeed, XRD analysis of Cu-S after SCR testing reveals that this sample becomes completely amorphous. Obviously, during SCR testing, or during the pretreatment (sample held in a 14% O_2/N_2 flow for 1h at 500 °C), the CHA structure of Cu-S collapsed. Surface area/pore volume analyses reveal that the Cu-S sample has a BET surface area of 87 m^2/g and a micropore volume of 0.042 cm^3/g ; these values are much smaller than the corresponding values for Cu-F and are thus consistent with a collapsed CHA structure. Note that

prior to surface area/pore volume analyses, hydrated ambient Cu-S was treated at 250 °C in high vacuum overnight. Obviously, such a treatment also induces CHA structure collapse.

To better understand the SAPO-34 structural degradation, in situ dehydration of the hydrated Cu-S samples was conducted in a variable temperature XRD apparatus under flowing dry N₂. As shown in Figure 2, while the hydrated Cu-S sample maintains the CHA structure at ambient temperatures, the CHA structure collapses irreversibly at temperatures above ~80 °C, i.e., when extensive dehydration starts to occur. This result indicates that during storage, the SAPO-34 framework must have undergone extensive hydrolysis of the ≡Si-O(H)-Al≡ bonds to form terminal ≡Si-OH, ≡Al(H₂O)₃ and/or other dangling moieties. The maintenance of the CHA structure in storage is due presumably to kinetic effects; i.e., the space-filling role of absorbed H₂O prevents condensation reactions between such dangling moieties that lead to crystallinity loss. However, when the space-filling water molecules are thermally driven out of the CHA pores, CHA structure collapse becomes inevitable. The XRD result shown in Figure 2 suggests that the Cu-S sample will certainly lose its crystallinity during pretreatment at 500 °C prior to SCR testing. Therefore, its poor SCR performance as shown in Figure 1 is nicely explained.

However, commercial Cu/SAPO-34 SCR catalysts, particularly catalysts synthesized using SAPO-34 supports formed with SDAs other than morpholine, do not show the type of dramatic structural degradation following a heat treatment after storage as described above. In fact, some “dead” commercial Cu/SAPO-34 catalysts maintain very decent CHA structural integrity. Therefore, there must exist a mechanism where only minor structural degradation of the SAPO-34 support necessitates conversion of SCR active Cu(II)-ions to SCR inactive Cu-containing moieties. Next, H₂-TPR was used to elucidate the nature of the SCR inactive Cu-containing moieties in Cu-S *after* its CHA structure collapse. Following that, we further suggest possible reaction pathways

that lead to Cu-ion deactivation *before* CHA structure collapse based on NMR and EPR investigations.

The nature of the Cu species in the Cu-F and Cu-S catalysts were compared using H₂-TPR to probe their reducibility. No dehydration treatment was performed prior to TPR to avoid any autoreduction of the catalysts. For the Cu-F sample, Cu reduction commences at ~150 °C, peaks at ~245 °C, and a less resolved shoulder peak extends above 300 °C as shown in Figure 3. In contrast, the Cu-S sample is much more difficult to reduce, as evidenced by the broad reduction peak centered at ~365 °C. Using Ag₂O reduction as a calibration, reduction peak areas between 100-600 °C were integrated and ratioed against the amount of Cu in the samples. This quantification gives H/Cu atomic ratios of 1.63±0.16 for Cu-F and 1.98±0.08 for Cu-S. On the basis of literature assignments [2, 9], the ~245 °C reduction state for Cu-F is readily attributed to Cu(II) → Cu(I) reduction for isolated Cu ions, while the higher temperature shoulder feature can be assigned to Cu(I) → Cu(0). The quantification result indicates that certain Cu(I) ions in Cu-F are stable and will require temperatures higher than 600 °C to reduce. For the Cu-S sample, reduction centered at ~365 °C is readily assigned to Cu(II) → Cu(0) reduction based on the H/Cu quantification described just above. Moreover, the rather high reduction temperature suggests that the Cu moieties in this sample are no longer isolated Cu(II) ions in cationic positions. Rather, the reduction temperature matches very well with reduction of copper aluminate-like species generated during hydrothermal treatment of Cu/zeolites [33]. As indicated by in situ Cu-S dehydration data shown in Figure 2, it is evident that the CHA structure of hydrated Cu-S must have collapsed prior to extensive Cu(II) reduction during H₂-TPR. Based on this, we assign the Cu moieties in post-CHA structure-collapsed Cu-S to CuAl₂O₄-like species. It becomes critically important, however, to elucidate whether CuAl₂O₄-like species form concomitant to CHA

structural collapse, or prior to that (i.e., during storage). In our recent publication [27], we suggested that a precursor to CuAl_2O_4 -like species forms prior to CHA structural collapse via a series of H_2O -assisted chemistries that include (1) hydrolysis of Brønsted acid sites of the SAPO-34 support, (2) hydrolysis of the SCR active site $[\text{Cu}(\text{OH})]^+$ to $\text{Cu}(\text{OH})_2$, and (3) interaction between terminal Al and $\text{Cu}(\text{OH})_2$ to form precursors for CuAl_2O_4 -like species. In the next, we provide spectroscopic data to suggest that these chemistries occur at ambient temperature, and do not necessarily require extensive structural degradation of the SAPO-34 support.

The most informative technique for elucidating local SAPO-34 framework structural changes is solid-state NMR. As such, these methods were used to obtain and compare ^{27}Al , ^{29}Si and ^{31}P MAS NMR spectra of hydrated Cu-F and Cu-S (prior to its CHA structural collapse). As shown in Figure 4(a), ^{27}Al signals centered at ~ 43 ppm are assigned to tetrahedrally coordinated framework aluminum atoms. Peaks at ~ -9 ppm are attributed to octahedrally coordinated Al; e.g., framework Al coordinated with two H_2O molecules, or extraframework Al species [21, 34]. Deconvoluted peak area comparisons (signals mass normalized) demonstrate that the Cu-F sample contains higher concentrations of tetrahedrally coordinated Al than Cu-S; i.e., the Cu-S sample is more defective. This can be attributed to hydrolysis of some of the $\equiv\text{Si}-\text{O}(\text{H})-\text{Al}\equiv$ moieties during storage [20, 35]. As shown in Figure 4(b), both samples contain two prominent ^{29}Si features at -90 and -111 ppm, respectively. The former peak is assigned to framework Si with 4 Al in the first coordination sphere (i.e., $\text{Si}(\text{OAl})_4$), and the latter to Si with 4 Si nearest neighbors as silica islands (i.e., $\text{Si}(\text{OSi})_4$) [21, 34]. The presence of weaker $\text{Si}(\text{OAl})_x(\text{OSi})_{4-x}$ resonances between these two prominent features in the spectra are not clearly resolved but cannot be ruled out. The $\text{Si}(\text{OAl})_4$ resonance of the Cu-S sample appears to be broader than that for Cu-F; in particular, a shoulder feature appearing at ~ 86 ppm (marked with an asterisk), attributable to tetrahedrally coordinated

Si(OAl)₄ species with disordered local structures [20, 36], is evident. This again indicates that this sample is more defective. From Figure 4(c), the -27 ppm ³¹P resonance is attributed to framework P with 4 Al in the first coordination sphere (i.e., P(OAl)₄). The resonance at -16 ppm can be assigned to hydrated (i.e., P(OAl)₄(H₂O)_x), or defective (i.e., P(OAl)_{4-x}(H₂O)_x) P species [21, 35, 37]. The relative signal intensity comparison between the two samples is again consistent with a defective nature for Cu-S. Overall, the comparison between NMR spectra of Cu-F and Cu-S indicates the latter sample experiences extensive ≡Si-O(H)-Al≡ hydrolysis from water attack. Such a hydrolysis chemistry generates terminal ≡Si-OH and ≡Al(H₂O)₃ species. Framework T sites next to such terminal Si and Al sites also become “defective”, displaying unique resonances different from their regular T site counterparts.

To fully understand whether the “defective” SAPO-34 support is capable of transforming SCR active Cu-ions into SCR inactive Cu-moieties (i.e., precursors to CuAl₂O₄-like species) during ambient temperature storage, a non-destructive technique that is capable to probing isolated Cu species and their surroundings must be used. As has been described above, any heat treatment above ~100 °C will cause irreversible collapse of the hydrated Cu-S sample (Figure 2). In this regard, a pulsed EPR technique, hyperfine sublevel correlation (HYSCORE), is ideal for such measurements [27]: (1) HYSCORE probes coupling between a EPR active species (isolated Cu(II) here) and its NMR active neighboring nuclei (²⁷Al and ¹H here) within a range of 0.25-0.8 nm; (2) measurements are done on hydrated samples at 10 K, therefore no damage of the hydrated Cu-S structure is anticipated. Upon acquiring the spectra, extensive HYSCORE simulations were performed based on the “saffron” function in EasySpin, a Matlab package for spectral simulation and analysis in EPR [38]. First, an experimental HYSCORE spectrum was separated into ¹H and ²⁷Al regions and normalized individually. The experimental parameters, such as magnetic field,

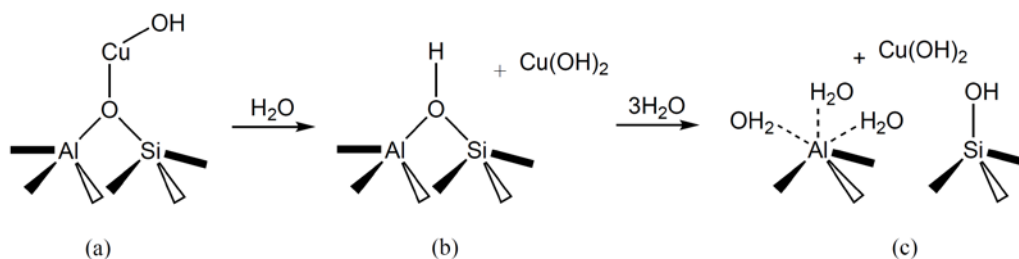
excitation frequency, number of points, dwell time, pulse width, and pulse delay, were copied directly from the HYSCORE experiments, while axial g tensor values and hyperfine parameters of Cu were obtained using the least-squares fitting program, “esfit”, in EasySpin by fitting the experimental solid-state continuous wave (CW) EPR spectra. More details regarding the simulations can be found in the supporting information of Ref. [27].

Figure 5 shows surface plots of HYSCORE spectra of the four samples: hydrated and dehydrated Cu-F, and hydrated and dehydrated Cu-S. In these spectra, signals in the lower field are attributed to Cu···Al coupling and features at higher field are attributed to Cu···H coupling. Note that quantitative signal intensity comparison between different spectra requires mass and gain normalization, which gives normalized intensity ratio of hydrated Cu-F: hydrated Cu-S: dehydrated Cu-F: dehydrated Cu-S = 1: 0.07: 0.02: 0.01. Were all spectra plotted using the same scale, the dehydrated samples would have been essentially featureless. Therefore, the spectra in Figure 5 are plotted in such a way that each spectrum is normalized against its own strongest Cu···Al coupling peak. In this case, signal intensity comparison between different spectra is only meaningful when corrected using the normalized intensity ratios shown above. Important information obtained from the experiments and simulations are summarized as follows:

(1) Cu···H coupling is observed in hydrated and dehydrated Cu-F, and hydrated Cu-S. This feature is not observed in dehydrated Cu-S. For the three samples with detectable Cu···H coupling, the simulated Cu-H distances are all 2.48 Å indicating that in all cases, it is the Cu-OH species that gives rise to Cu···H coupling.

(2) In terms of Cu···Al coupling, simulations suggest the presence of three types of such coupling: (i) Cu(II) adjacent to a single Al nucleus with a Cu-Al distance of 2.74 Å; (ii) Cu(II) close to two Al nuclei both with a Cu-Al distance of 2.74 Å and the vectors connecting Cu and the

two Al are 52° apart; (iii) Cu(II) further away from Al with Cu-Al distances greater than 5 \AA . In hydrated Cu-F, type (i) dominates. Upon Cu-F dehydration, contribution from type (ii) increases, resulting in splitting of the Cu \cdots Al coupling signal. For hydrated Cu-S, interestingly, the signal largely comes from type (iii) coupling. This is very important, suggesting that during storage, the isolated Cu species move away from framework Al. Next, we propose that this is due to the occurrence of a series of hydrolysis reactions that are schematically shown in Scheme 1 below:



Scheme 1. hydrolysis reactions of the SCR active site $\text{Cu}(\text{OH})^+$ and the regenerated Brønsted acid site

Structure (a) shown in Scheme 1 denotes the SCR active $[\text{Cu}(\text{OH})]^+$ site in Cu-F. EPR simulated Cu-H and Cu-Al distances of 2.48 and 2.74 \AA , respectively, are consistent with distances calculated with DFT [27]. With the assistance from water molecules trapped in CHA cages, hydrolysis of the O-Cu bond lead to formation of a free $\text{Cu}(\text{OH})_2$ molecule and the regeneration of a Brønsted acid site $\equiv\text{Al-O}(\text{H})\text{-Si}\equiv$ (i.e., structure (b)). The Brønsted acid site can further hydrolyze to structure (c). Note that these chemistries are fully consistent with our experimental observations: (1) the as-formed free $\text{Cu}(\text{OH})_2$ molecule is still EPR active, consistent with the fact that hydrated Cu-S still contains 0.51 wt\% EPR detectable Cu; (2) the distance increase between Al and Cu greatly lowers effective coupling between these two moieties, leading to a dramatic decrease of the HYSORE signal intensity for Cu-S as compared to Cu-F. Indeed, as suggested by HYSORE simulations, Al and Cu distances in hydrated Cu-S is larger than 5 \AA .

What is not included in scheme 1, is how $\equiv\text{Al}(\text{H}_2\text{O})_3$ and $\text{Cu}(\text{OH})_2$ interact with each other to form CuAl_2O_4 -like species upon Cu-S dehydration (or calcination). In our recent study, we proposed via DFT simulations that this chemistry occurs through a double-bridged $=\text{Al}(\mu\text{-O}_2)\text{Cu}$ intermediate [27]. We note that the precise structure of the CuAl_2O_4 -like species in chabazite is not yet determined. As shown in Figure 6(D), $\text{Cu}\cdots\text{Al}$ coupling is still readily detectable in dehydrated Cu-S, however $\text{Cu}\cdots\text{H}$ coupling is no longer detected. Therefore, in CuAl_2O_4 -like species, Cu appears to stay close to Al (likely with the formation of Cu-O-Al linkages), but -OH groups appear not to bond to Cu anymore.

Finally, we note again that in order to study low-temperature Cu/SAPO-34 deactivation, a model catalyst particularly vulnerable to water attack is used in this study. Industrial Cu/SAPO-34 SCR catalysts are much more stable, and even some fully deactivated ones maintain the chabazite structure. We argue here, however, the deactivation mechanism derived in the present study, i.e., hydrolysis chemistry induced transformation of SCR active Cu to CuAl_2O_4 -like species, is generally applicable to all Cu/SAPO-34 catalysts. Our rationale is that such a Cu transformation mechanism is realized with very minor local damage of the SAPO-34 support, leading to the typical symptom of a deactivated industrial Cu/SAPO-34 SCR catalyst, i.e., the CHA structure appears intact however the catalyst no longer catalyzes SCR effectively.

4. Conclusions

A one-pot catalyst synthesis method, using Cu-TEPA as the Cu carrier and co-SDA, allows for the preparation of low Cu-loaded model Cu/SAPO-34 SCR catalysts with essentially all Cu present as isolated Cu(II) ions. Following extended storage on the shelf under ambient laboratory conditions, this catalyst lost essentially all of its SCR activity due to two slow, ambient temperature processes aided by condensed water in the zeolite pores. These are: (1) hydrolysis reactions of $\equiv\text{Si}$ -

O(H)-Al≡ bonds causing the SAPO-34 framework to become defective; and (2) detachment of Cu from cationic exchange positions, and its subsequent interaction with active Al moieties (e.g., ≡Al(H₂O)₃) to form SCR inactive CuAl₂O₄-like species. Even though SAPO-34 structural collapse aggravates catalyst deactivation, formation of CuAl₂O₄-like species is ultimately responsible for SCR activity loss.

Acknowledgements

The authors gratefully acknowledge the US Department of Energy (DOE), Energy Efficiency and Renewable Energy, Vehicle Technologies Office for the support of this work. The experimental studies described in this paper were performed in the William R. Wiley Environmental Molecular Sciences Laboratory (EMSL), a national scientific user facility located at Pacific Northwest National Laboratory (PNNL). PNNL is operated by Battelle for the US DOE under contract DE-AC05-76RL01830.

References:

- [1] R. Martinez-Franco, M. Moliner, C. Franch, A. Kustov, A. Corma, Rational direct synthesis methodology of very active and hydrothermally stable Cu-SAPO-34 molecular sieves for the SCR of NO_x, *Appl Catal B-Environ*, 127 (2012) 273-280.
- [2] J. Wang, T. Yu, X.Q. Wang, G.S. Qi, J.J. Xue, M.Q. Shen, W. Li, The influence of silicon on the catalytic properties of Cu/SAPO-34 for NO_x reduction by ammonia-SCR, *Appl Catal B-Environ*, 127 (2012) 137-147.
- [3] L. Wang, W. Li, G.S. Qi, D. Weng, Location and nature of Cu species in Cu/SAPO-34 for selective catalytic reduction of NO with NH₃, *J Catal*, 289 (2012) 21-29.
- [4] S.K. Fan, J.J. Xue, T. Yu, D.Q. Fan, T. Hao, M.Q. Shen, W. Li, The effect of synthesis methods on Cu species and active sites over Cu/SAPO-34 for NH₃-SCR reaction, *Catal Sci Technol*, 3 (2013) 2357-2364.
- [5] F. Gao, E.D. Walter, N.M. Washton, J. Szanyi, C.H.F. Peden, Synthesis and Evaluation of Cu-SAPO-34 Catalysts for Ammonia Selective Catalytic Reduction. 1. Aqueous Solution Ion Exchange, *Acs Catal*, 3 (2013) 2083-2093.
- [6] P.N.R. Vennestrom, A. Katerinopoulou, R.R. Tiruvalam, A. Kustov, P.G. Moses, P. Concepcion, A. Corma, Migration of Cu Ions in SAPO-34 and Its Impact on Selective Catalytic Reduction of NO_x NH₃, *Acs Catal*, 3 (2013) 2158-2161.
- [7] D. Wang, L. Zhang, K. Kamasamudram, W.S. Epling, In Situ-DRIFTS Study of Selective Catalytic Reduction of NO_x by NH₃ over Cu-Exchanged SAPO-34, *Acs Catal*, 3 (2013) 871-881.
- [8] L. Wang, J.R. Gaudet, W. Li, D. Weng, Migration of Cu species in Cu/SAPO-34 during hydrothermal aging, *J Catal*, 306 (2013) 68-77.

- [9] J.J. Xue, X.Q. Wang, G.S. Qi, J. Wang, M.Q. Shen, W. Li, Characterization of copper species over Cu/SAPO-34 in selective catalytic reduction of NO_x with ammonia: Relationships between active Cu sites and de-NO_x performance at low temperature, *J Catal*, 297 (2013) 56-64.
- [10] T. Yu, J. Wang, M.Q. Shen, W. Li, NH₃-SCR over Cu/SAPO-34 catalysts with various acid contents and low Cu loading, *Catal Sci Technol*, 3 (2013) 3234-3241.
- [11] D. Wang, L. Zhang, J.H. Li, K. Kamasamudram, W.S. Epling, NH₃-SCR over Cu/SAPO-34 - Zeolite acidity and Cu structure changes as a function of Cu loading, *Catal Today*, 231 (2014) 64-74.
- [12] J. Wang, Y. Huang, T. Yu, S.C. Zhu, M.Q. Shen, W. Li, J.Q. Wang, The migration of Cu species over Cu-SAPO-34 and its effect on NH₃ oxidation at high temperature, *Catal Sci Technol*, 4 (2014) 3004-3012.
- [13] T. Yu, D.Q. Fan, T. Hao, J. Wang, M.Q. Shen, W. Li, The effect of various templates on the NH₃-SCR activities over Cu/SAPO-34 catalysts, *Chem Eng J*, 243 (2014) 159-168.
- [14] F. Gao, E.D. Walter, N.M. Washton, J. Szanyi, C.H.F. Peden, Synthesis and evaluation of Cu/SAPO-34 catalysts for NH₃-SCR 2: Solid-state ion exchange and one-pot synthesis, *Appl Catal B-Environ*, 162 (2015) 501-514.
- [15] K. Leistner, L. Olsson, Deactivation of Cu/SAPO-34 during low-temperature NH₃-SCR, *Appl Catal B-Environ*, 165 (2015) 192-199.
- [16] J. Wang, D.Q. Fan, T. Yu, J.Q. Wang, T. Hao, X.Q. Hu, M.Q. Shen, W. Li, Improvement of low-temperature hydrothermal stability of Cu/SAPO-34 catalysts by Cu²⁺ species, *J Catal*, 322 (2015) 84-90.
- [17] D. Wang, Y. Jangjou, Y. Liu, M.K. Sharma, J.Y. Luo, J.H. Li, K. Kamasamudram, W.S. Epling, A comparison of hydrothermal aging effects on NH₃-SCR of NO_x over Cu-SSZ-13 and Cu-SAPO-34 catalysts, *Appl Catal B-Environ*, 165 (2015) 438-445.
- [18] K. Leistner, O. Mihai, K. Wijayanti, A. Kumar, K. Kamasamudram, N.W. Currier, A. Yezerets, L. Olsson, Comparison of Cu/BEA, Cu/SSZ-13 and Cu/SAPO-34 for ammonia-SCR reactions, *Catal Today*, 258 (2015) 49-55.
- [19] J. Woo, K. Leistner, D. Bernin, H. Ahari, M. Shost, M. Zammit, L. Olsson, Effect of various structure directing agents (SDAs) on low-temperature deactivation of Cu/SAPO-34 during NH₃-SCR reaction, *Catal Sci Technol*, 8 (2018) 3090-3106.
- [20] M. Briend, R. Vomscheid, M.J. Peltre, P.P. Man, D. Barthomeuf, INFLUENCE OF THE CHOICE OF THE TEMPLATE ON THE SHORT-TERM AND LONG-TERM STABILITY OF SAPO-34 ZEOLITE, *J. Phys. Chem.*, 99 (1995) 8270-8276.
- [21] A. Buchholz, W. Wang, A. Arnold, M. Xu, M. Hunger, Successive steps of hydration and dehydration of silicoaluminophosphates H-SAPO-34 and H-SAPO-37 investigated by in situ CF MAS NMR spectroscopy, *Micropor Mesopor Mat*, 57 (2003) 157-168.
- [22] T. Fjermestad, S. Svelle, O. Swang, Mechanistic Comparison of the Dealumination in SSZ-13 and the Desilication in SAPO-34, *J Phys Chem C*, 117 (2013) 13442-13451.
- [23] J. Song, Y.L. Wang, E.D. Walter, N.M. Washton, D.H. Mei, L. Kovarik, M.H. Engelhard, S. Prodingler, Y. Wang, C.H.F. Peden, F. Gao, Toward Rational Design of Cu/SSZ-13 Selective Catalytic Reduction Catalysts: Implications from Atomic-Level Understanding of Hydrothermal Stability, *Acs Catal*, 7 (2017) 8214-8227.
- [24] F. Gao, J. Szanyi, On the hydrothermal stability of Cu/SSZ-13 SCR catalysts, *Appl Catal a-Gen*, 560 (2018) 185-194.
- [25] F. Gao, C.H.F. Peden, Recent Progress in Atomic-Level Understanding of Cu/SSZ-13 Selective Catalytic Reduction Catalysts, *Catalysts*, 8 (2018) 140.
- [26] Y. Cao, D. Fan, P. Tian, L. Cao, T.T. Sun, S.T. Xu, M. Yang, Z.M. Liu, The influence of low-temperature hydration methods on the stability of Cu-SAPO-34 SCR catalyst, *Chem Eng J*, 354 (2018) 85-92.
- [27] A.Y. Wang, Y. Chen, E.D. Walter, N.M. Washton, D.H. Mei, T. Varga, Y.L. Wang, J. Szanyi, Y. Wang, C.H.F. Peden, F. Gao, Unraveling the mysterious failure of Cu/SAPO-34 selective catalytic reduction catalysts, *Nat Commun*, 10 (2019).

- [28] A.M. Prakash, S. Unnikrishnan, Synthesis of Sapo-34 - High-Silicon Incorporation in the Presence of Morpholine as Template, *J Chem Soc Faraday T*, 90 (1994) 2291-2296.
- [29] R. Martinez-Franco, M. Moliner, P. Concepcion, J.R. Thogersen, A. Corma, Synthesis, characterization and reactivity of high hydrothermally stable Cu-SAPO-34 materials prepared by "one-pot" processes, *J Catal*, 314 (2014) 73-82.
- [30] F. Gao, E.D. Walter, M. Kollar, Y.L. Wang, J. Szanyi, C.H.F. Peden, Understanding ammonia selective catalytic reduction kinetics over Cu/SSZ-13 from motion of the Cu ions, *J Catal*, 319 (2014) 1-14.
- [31] F. Gao, E.D. Walter, E.M. Karp, J.Y. Luo, R.G. Tonkyn, J.H. Kwak, J. Szanyi, C.H.F. Peden, Structure-activity relationships in NH₃-SCR over Cu-SSZ-13 as probed by reaction kinetics and EPR studies, *J Catal*, 300 (2013) 20-29.
- [32] Y.J. Kim, J.K. Lee, K.M. Min, S.B. Hong, I.S. Nam, B.K. Cho, Hydrothermal stability of CuSSZ13 for reducing NO_x by NH₃, *J Catal*, 311 (2014) 447-457.
- [33] P.N.R. Vennestrom, T.V.W. Janssens, A. Kustov, M. Grill, A. Puig-Molina, L.F. Lundegaard, R.R. Tiruvalam, P. Concepcion, A. Corma, Influence of lattice stability on hydrothermal deactivation of Cu-ZSM-5 and Cu-IM-5 zeolites for selective catalytic reduction of NO_x by NH₃, *J Catal*, 309 (2014) 477-490.
- [34] J. Tan, Z.M. Liu, X.H. Bao, X.C. Liu, X.W. Han, C.Q. He, R.S. Zhai, Crystallization and Si incorporation mechanisms of SAPO-34, *Micropor Mesopor Mat*, 53 (2002) 97-108.
- [35] R. Vomscheid, M. Briend, M.J. Peltre, P. Massiani, P.P. Man, D. Barthomeuf, Reversible Modification of the Si Environment in Template-Free Sapo-34 Structure Upon Hydration Dehydration Cycles Below Ca 400k, *J Chem Soc Chem Comm*, (1993) 544-546.
- [36] J.A. Martens, P.J. Grobet, P.A. Jacobs, Catalytic Activity and Si, Al, P Ordering in Microporous Silicoaluminophosphates of the Sapo-5, Sapo-11, and Sapo-37 Type, *J Catal*, 126 (1990) 299-305.
- [37] Y. Watanabe, A. Koiwai, H. Takeuchi, S.A. Hyodo, S. Noda, Multinuclear Nmr-Studies on the Thermal-Stability of Sapo-34, *J Catal*, 143 (1993) 430-436.
- [38] S. Stoll, A. Schweiger, EasySpin, a comprehensive software package for spectral simulation and analysis in EPR, *Journal of Magnetic Resonance*, 178 (2006) 42-55.

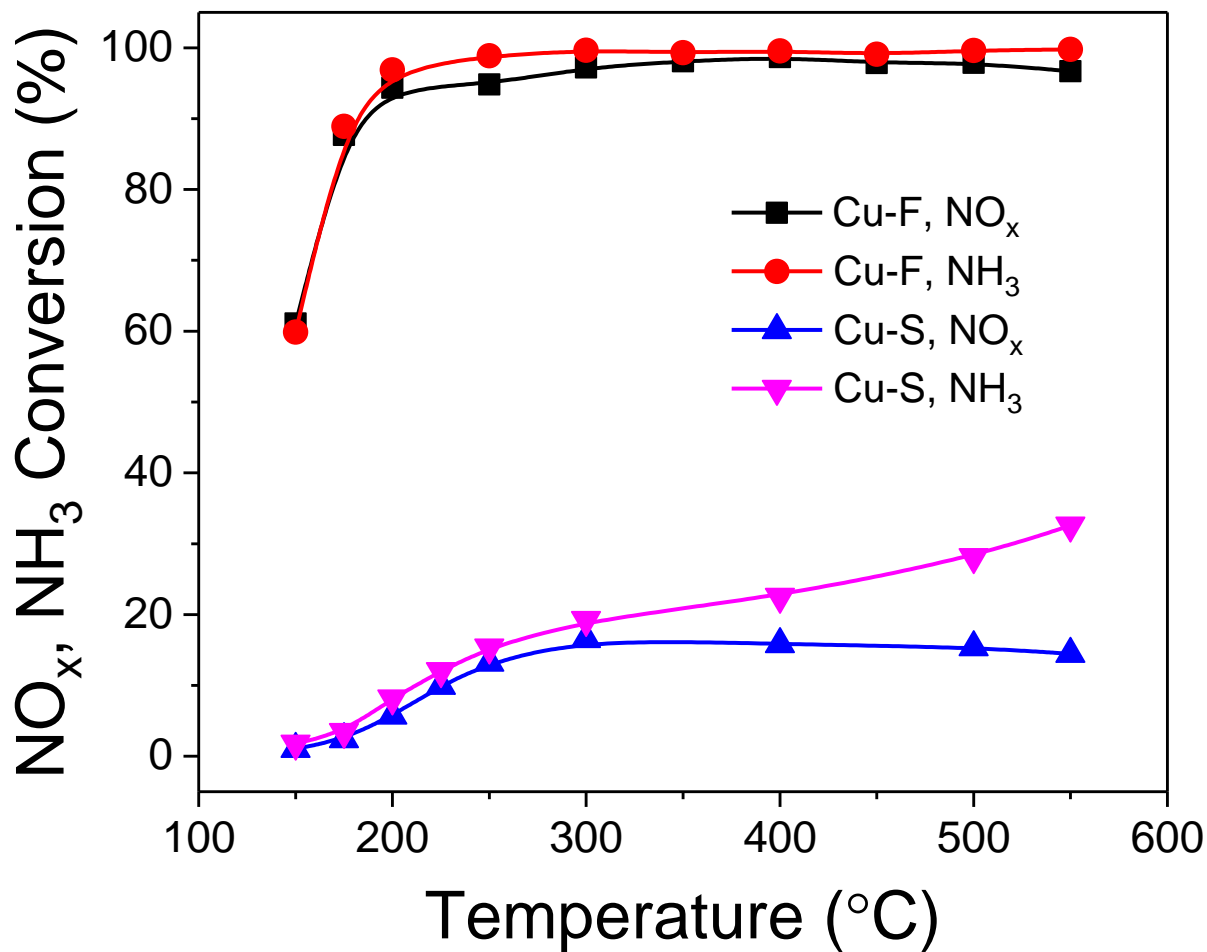


Figure 1. NO_x and NH₃ conversions versus temperature curves for Cu-F and Cu-S samples in standard SCR. The feed gas contained 360 ppm NO, 360 ppm NH₃, 14% O₂, 2.5% H₂O and balance N₂. The total gas flow was 1000 sccm, and the gas hourly space velocity (GHSV) was calculated to be ~200,000 h⁻¹ for a catalyst amount of 200 mg.

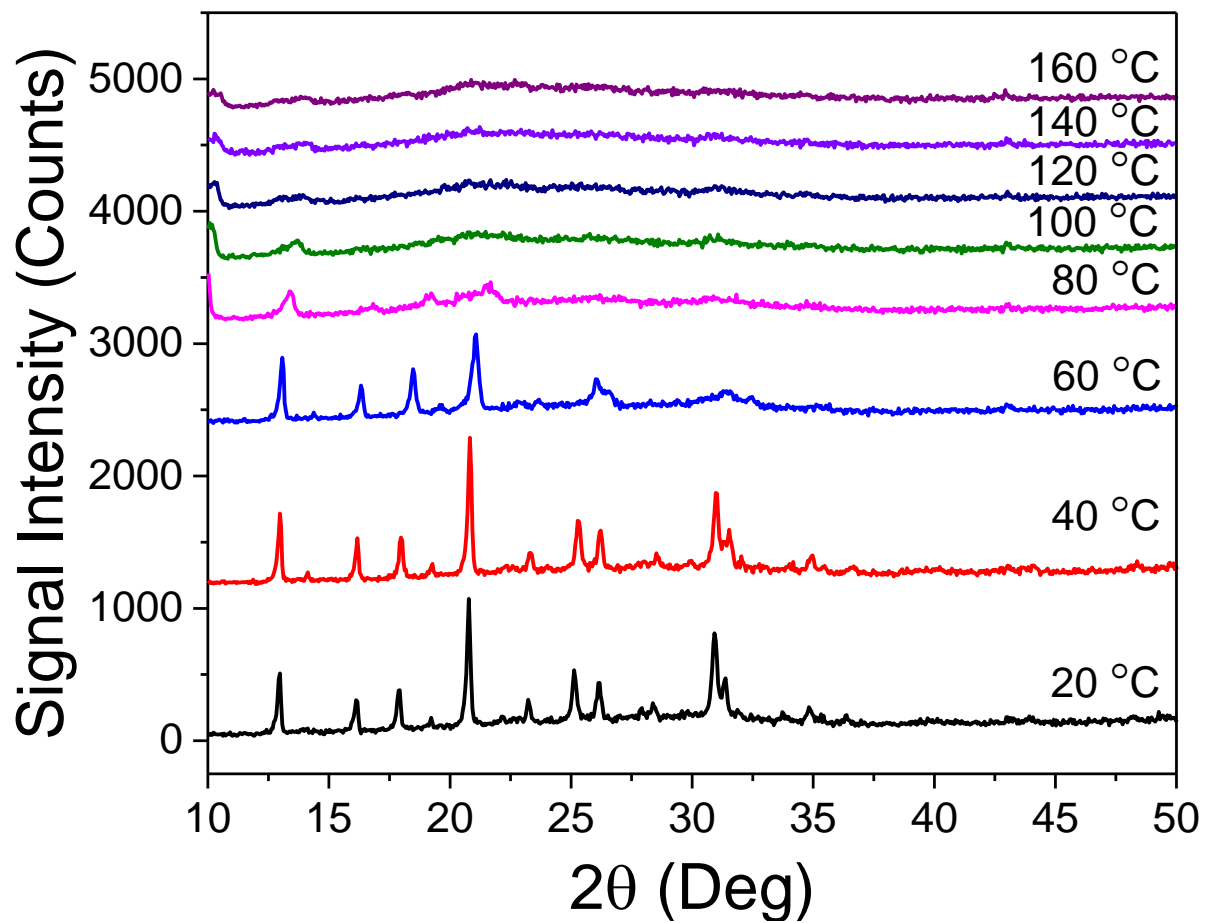


Figure 2. XRD patterns for the Cu-S sample during *in situ* dehydration.

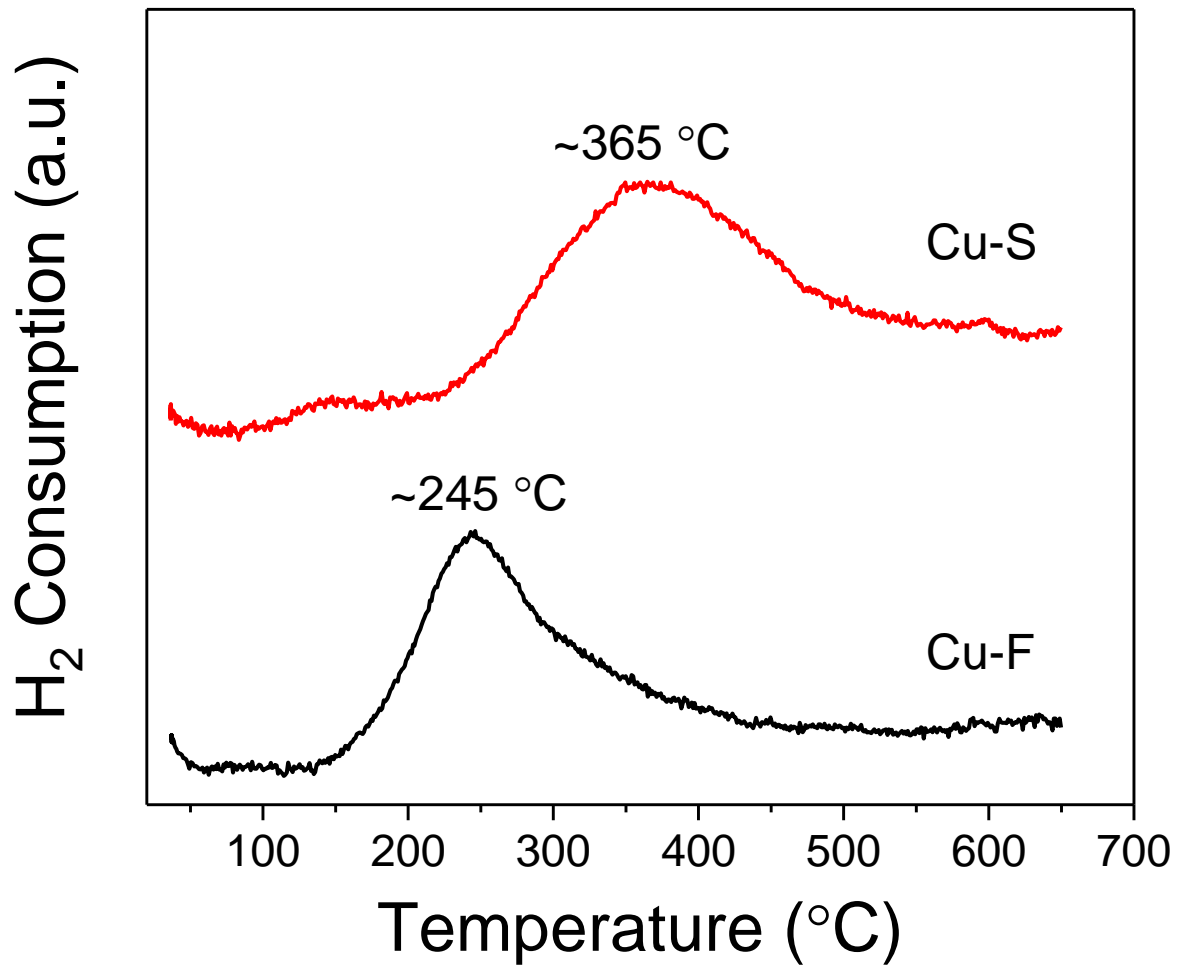


Figure 3. H₂-TPR results for Cu-F and Cu-S samples.

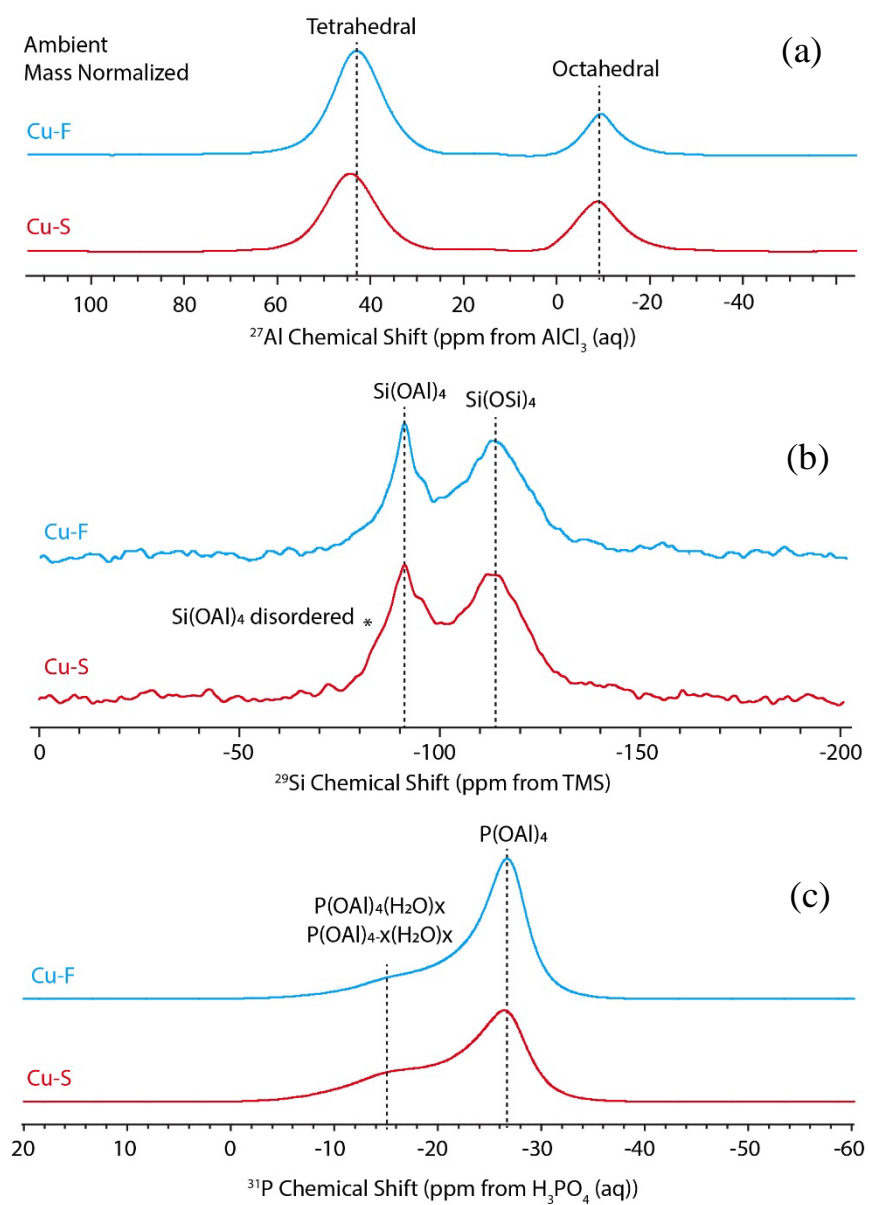


Figure 4. (a) ^{27}Al , (b) ^{29}Si , and (c) ^{31}P solid-state NMR spectra for hydrated ambient Cu-F and Cu-S samples. All spectra are mass normalized for the purpose of direct comparison.

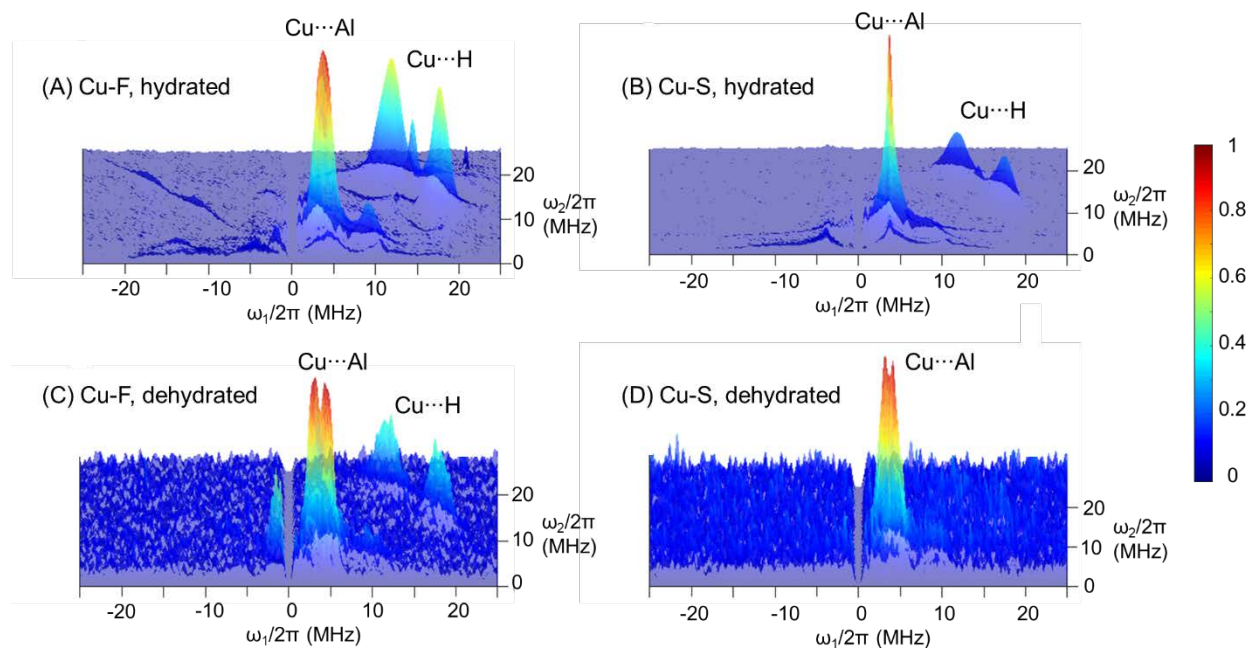


Figure 5. Surface plots of HYSCORE experimental spectra for hydrated Cu-F (A) and Cu-S (B) as well as dehydrated Cu-F (A) and Cu-S (B) samples. All spectra are normalized by their maximum peak at Cu···Al interaction region. Note that the signal to noise ratio is relatively low for the dehydrated samples compared to the hydrated samples primarily due to the slower molecular mobility with the loss of water. The mass and gain normalized intensity ratio of hydrated Cu-F: hydrated Cu-S: dehydrated Cu-F: dehydrated Cu-S = 1: 0.07: 0.02: 0.01.